Nonlocality in Imaging

M. P. Oxley, E. C. Cosgriff, and L. J. Allen
School of Physics, University of Melbourne, Victoria 3010, Australia
(Received 6 March 2005; published 26 May 2005)

We show how an effective nonlocality in imaging can lead to the sampling of a spatial region which is not significantly illuminated by an imaging probe. The nonlocality is embodied in the effective nonlocal potential describing inelastic scattering which occurs when coupled channel Schrödinger equations are reduced to a single integro-differential equation. The context in which this prediction will be illustrated is atomic resolution imaging based on energy-loss spectroscopy in scanning transmission electron microscopy.

DOI: 10.1103/PhysRevLett.94.203906 PACS numbers: 42.30.Va, 61.14.Dc

Since the 1964 analysis of John Bell (Bell's theorem) it is widely recognized that quantum theory is nonlocal in the sense that there is no way for the results in one region of space to be independent of choices made in another spatially separated region [1]. In this Letter we predict and elucidate an analogous phenomenon where it is demonstrated that an effective nonlocality in imaging can lead to the sampling of a spatial region *which is effectively not illuminated by an imaging probe*.

The context in which this phenomenon will be illustrated is atomic resolution imaging based on electron energy-loss spectroscopy (EELS) in scanning transmission electron microscopy (STEM) [2,3], specifically core-loss spectroscopy of weakly bound electrons. The theoretical framework in which such imaging is described starts with the Schrödinger equation [4,5]

$$\left[\frac{-\hbar^2}{2m}\nabla^2 + H(\tau) + H'(\mathbf{r};\tau)\right]\Psi(\mathbf{r};\tau) = E\Psi(\mathbf{r};\tau), \quad (1)$$

where $\mathbf{r}$ is the coordinate of the incident electron and $\tau \equiv \{\mathbf{r}_1, \ldots, \mathbf{r}_N\}$ denotes the coordinates of the particles (nuclei or electrons) in the specimen being imaged. The term $H(\tau)$ is the Hamiltonian for all the particles in the specimen and $H'(\mathbf{r};\tau)$ describes the interaction of the incident electron with the particles in the specimen. The total energy of the system $E = E_0 + \varepsilon_0$, where E_0 is the energy of the incident electron in vacuum and ε_0 is the initial energy of the specimen. We assume the wave function can be expanded in the form

$$\Psi(\mathbf{r};\tau) = \sum_n \psi_n(\mathbf{r})a_n(\tau). \quad (2)$$

The normalized wave function $a_n(\tau)$ represents the nth stationary state of the specimen (of energy ε_n) and satisfies $H(\tau)a_n(\tau) = \varepsilon_n a_n(\tau)$. The initial state is denoted $a_0(\tau)$, with $\psi_0(\mathbf{r})$ then describing the elastic scattering. Furthermore $\psi_n(\mathbf{r})(n \neq 0)$ describes the inelastic scattering by which the state of the specimen is changed from $a_0(\tau)$ to $a_n(\tau)$. The energy associated with $\psi_n(\mathbf{r})$, i.e., after the inelastic scattering event, is $E_n = E - \varepsilon_n \equiv h^2k_n^2/2m$, where k_n is the magnitude of the wave vector of the scattered electron. The energy loss of the incident fast electron after an inelastic scattering event which excites the crystal from the initial to the nth excited state is $E_{\text{loss}} = \varepsilon_n - \varepsilon_0$.

Using Eq. (2) we may recast Eq. (1) in the form of a set of coupled differential equations as follows:

$$\left[\nabla^2 + 4\pi^2k_n^2 - \frac{2m}{\hbar^2}H'_{nn}(\mathbf{r})\right]\psi_n(\mathbf{r}) = \frac{2m}{\hbar^2}\sum_{m\neq n}H'_{nm}(\mathbf{r})\psi_m(\mathbf{r}), \quad (3)$$

where

$$H'_{nm}(\mathbf{r}) = \int a_n^*(\tau)H'(\mathbf{r};\tau)a_m(\tau)d\tau. \quad (4)$$

We now make the common assumption that, in Eq. (3), only terms with $m = 0$ give a significant contribution, i.e., only excitations from the ground state contribute significantly to the scattering $[H'_{n0}(\mathbf{r}) \gg H_{nm}(\mathbf{r})(m \neq 0)]$. Then the set of coupled differential equations reduces to a single integro-differential equation of the form

$$\nabla^2\psi_0(\mathbf{r}) + \left[4\pi^2k_0^2 - \frac{2m}{\hbar^2}H'_{00}(\mathbf{r})\right]\psi_0(\mathbf{r}) - \frac{2m}{\hbar^2}\int A(\mathbf{r},\mathbf{r}')\psi_0(\mathbf{r}')d\mathbf{r}' = 0, \quad (5)$$

where the complex *nonlocal* kernel representing inelastic scattering of the fast electron is given by

$$A(\mathbf{r},\mathbf{r}') = -\frac{m}{2\pi\hbar^2}\sum_{m\neq 0}H'_{0m}(\mathbf{r})H'_{m0}(\mathbf{r}')\frac{e^{2\pi ik_m|\mathbf{r}-\mathbf{r}'|}}{|\mathbf{r}-\mathbf{r}'|}. \quad (6)$$

In STEM, imaging can be based on monitoring the cross section as a function of probe position $\mathbf{R}$ for inelastic scattering of a particular kind, for example, thermal diffuse scattering or electron core-loss spectroscopy. Using Eq. (5) and conservation of electron flux it can be shown that the cross section for the relevant inelastic scattering events can be written in the form [5]

$$\sigma(\mathbf{R}) = \frac{2\pi m}{h^2 k_0} \int_V \int_V \psi_0^*(\mathbf{R}, \mathbf{r}) W(\mathbf{r}, \mathbf{r}') \psi_0(\mathbf{R}, \mathbf{r}') d\mathbf{r} d\mathbf{r}', \tag{7}$$

where V is the volume of the specimen and

$$W(\mathbf{r}, \mathbf{r}') \equiv i[A(\mathbf{r}, \mathbf{r}') - A^*(\mathbf{r}', \mathbf{r})] \tag{8}$$

is an effective nonlocal potential representing the inelastic scattering. From Eq. (2.14) in Ref. [5] it follows, with some approximation and redefining the Fourier coefficients, that

$$W(\mathbf{r}, \mathbf{r}') = \frac{h^2 k_0}{2\pi m V} \sum_{\mathbf{h},\mathbf{g}} \mu_{\mathbf{h},\mathbf{g}} e^{2\pi i(\mathbf{k}_0 + \mathbf{h})\cdot\mathbf{r}} e^{-2\pi i(\mathbf{k}_0 + \mathbf{g})\cdot\mathbf{r}'}. \tag{9}$$

Here $\mathbf{g}$ and $\mathbf{h}$ are variables in the Fourier transform space. The coefficients $\mu_{\mathbf{h},\mathbf{g}}$ are the inelastic scattering coefficients, often referred to as the mixed dynamic form factors, the calculation of which is described in detail elsewhere [6,7]. We now assume that the incident electron beam has wave vector $\mathbf{k}_0$ in the z direction and also that we can make a projected potential approximation. Denoting a vector in the $x - y$ plane by $\mathbf{r}_\perp$, we may rewrite Eq. (7) in the form

$$\begin{aligned}\sigma(\mathbf{R}) = \frac{2\pi m}{h^2 k_0} & \int_0^t \int_0^t \exp[2\pi i k_0 (z - z')] \\ & \times \int_A \int_A \psi_0^*(\mathbf{R}, \mathbf{r}_\perp, z) W(\mathbf{r}_\perp, \mathbf{r}'_\perp) \psi_0(\mathbf{R}, \mathbf{r}'_\perp, z') \\ & \times d\mathbf{r}_\perp d\mathbf{r}'_\perp dz dz',\end{aligned} \tag{10}$$

for a slablike specimen of area A and thickness t and where the effective potential $W(\mathbf{r}_\perp, \mathbf{r}'_\perp)$ now has the form

$$W(\mathbf{r}_\perp, \mathbf{r}'_\perp) = \frac{h^2 k_0}{2\pi m A t} \sum_{\mathbf{h},\mathbf{g}} \mu_{\mathbf{h},\mathbf{g}} e^{2\pi i \mathbf{h}\cdot\mathbf{r}_\perp} e^{-2\pi i \mathbf{g}\cdot\mathbf{r}'_\perp}. \tag{11}$$

Incoherence of the contributions to the cross section from inelastic scattering at different atomic sites in the $x - y$ plane is catered for in the construction of the $\mu_{\mathbf{h},\mathbf{g}}$. We now enforce incoherence between different layers along the z direction [8] by inserting $t\delta(z - z')$ in Eq. (10). Insertion of the δ function on its own yields a cross section per unit length. The factor of t gives the cross section in units consistent with Eq. (7). We then obtain

$$\begin{aligned}\sigma(\mathbf{R}) = & \frac{2\pi m t}{h^2 k_0} \\ & \times \int_0^t \int_A \int_A \psi_0^*(\mathbf{R}, \mathbf{r}_\perp, z) W(\mathbf{r}_\perp, \mathbf{r}'_\perp) \psi_0(\mathbf{R}, \mathbf{r}'_\perp, z) \\ & \times d\mathbf{r}_\perp d\mathbf{r}'_\perp dz.\end{aligned} \tag{12}$$

This cross section can be evaluated in a multislice formulation by discretizing along the z direction. Doing this and using Eq. (11), Eq. (12) reduces to Eq. (A.7) in Ref. [9] (noting that the result there is a cross section per unit volume).

Let us now consider STEM using 200 keV electrons incident along the [011] zone axis of a slab of SiC, which we are illuminating with an aberration free probe formed using a 50 mrad aperture (planned for the next generation of microscopes). We calculate, using a frozen phonon model [9,10], the variation with probe position in the number of electrons which have ionized an electron in the C K shell and detected in an axial EELS detector with acceptance semiangle 10 mrad and an energy window of 40 eV. In Fig. 1(a) we show a line scan along the [100] direction. The locations of Si columns are indicated by gray circles and of C columns by black circles.

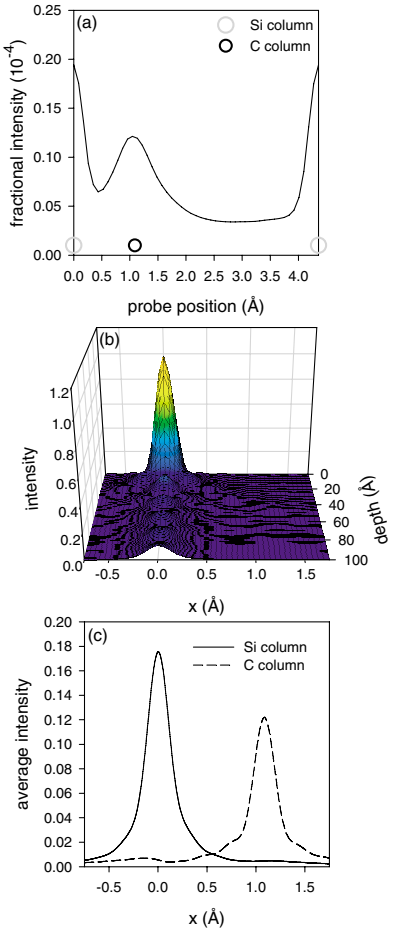

FIG. 1 (color online). (a) Simulated STEM image obtained by scanning along [100] with a 200 keV probe formed with a 50 mrad aperture and incident along the [011] zone axis of a 100 Å thick slab of SiC. Electrons that have ionized a K-shell electron in C are detected in an axial detector with acceptance semiangle of 10 mrad and an energy window of 40 eV. The result is expressed as a fraction of the incident electron flux, i.e., $\sigma(\mathbf{R})/A$. (b) Evolution of the intensity of the incident probe as a function of depth when the probe is positioned above the Si column. (c) The integral along z of the intensity shown in (b) (presented as an average) is compared with the integrated result obtained when the probe is above the C column.

When the probe is situated above the Si column then one is obtaining a signal which would usually be interpreted either as the presence of C atoms in that column or a strong ''cross talk'' signal from the adjacent C column. The former is not true and by the latter we mean that the probe has spread *significantly* onto the C column as it channels through the crystal. However, plotting the probe wave function within the crystal as a function of depth we find that this is simply not the case, as can be seen in Fig. 1(b). The integrated intensity for the probe on both the Si and C columns shown in Fig. 1(c) confirms this. We are in fact obtaining a larger signal on the Si column, when there is negligible (integrated) intensity on the C column, than when the probe is on the C column itself and there is considerable flux on that column.

How can this remarkable phenomenon be explained? We show that it is due to the nonlocal nature of the effective potential given by Eq. (11). This potential is hard to visualize; it is a four dimensional function. Therefore we will assume that the nonlocal potential varies only along the [100] direction and becomes a function of two variables only, denoted by $W(x, x')$. If we furthermore assume a probe which varies only along the x direction then the wave functions in Eq. (11) depend on x and x' respectively. Although this probe is somewhat artificial, it will allow us to understand the role of the nonlocality in the imaging process. With these assumptions, Eq. (12) reduces to the form

$$\sigma(R) = \frac{2\pi m t}{h^2 k_0} \times \int_0^t \iint \psi_0^*(R, x, z) W(x, x') \psi_0(R, x', z) dx dx' dz. \tag{13}$$

Under these conditions, for a probe generated with an ''aperture'' of 25 mrad, we obtain the image shown in Fig. 2(a), with all other parameters the same as in the previous case. Once again when the probe is on the Si column there is an unexpected strong K-loss signal from C. The probe's probability density on the C column, while more evident than for the zone axis case, is insufficient to account for this signal, as can be seen in Fig. 2(b). This is reinforced by comparison of the integrated intensity at the C column when the probe is on Si relative to that when the probe is actually on the C column, as illustrated in Fig. 2(c). Further evidence that the nonlocal nature of $W(x, x')$ is the key factor here (and not cross talk) is given in Fig. 2(d), where a STEM image is simulated for energy-dispersive x-ray analysis (EDX), where x rays are detected rather than energy-loss electrons. This is ''equivalent'' to an EELS experiment with a detector which subtends the whole solid angle and where electrons with energy losses over the whole possible range are detected. It is well known that under these conditions the effective ionization interaction can usually be approximated by a local potential [6],

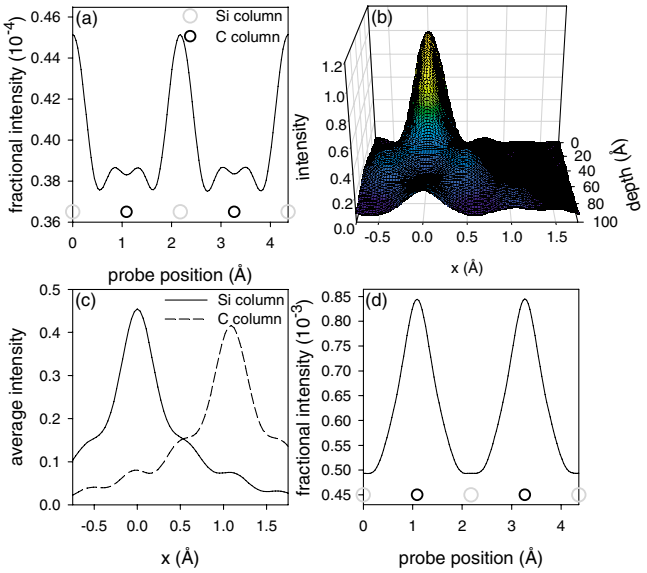

FIG. 2 (color online). (a) Simulated STEM image obtained by scanning along [100] with a 200 keV probe formed with a 25 mrad aperture and for [100] systematic row conditions on a 100 Å thick slab of SiC. Electrons that have ionized a K-shell electron in C are detected in an axial detector with acceptance angle of 10 mrad and an energy window of 40 eV. (b) Evolution of the probability density of the incident probe as a function of depth in the slab when the probe is positioned above the Si column. (c) The integral along z of the probability density shown in (b) is compared with the integrated result obtained when the probe is above the C column. (d) A STEM image obtained for the same conditions as in (a) except that the x rays arising from ionization are detected, rather than the energy-loss electrons.

i.e., $W(x, x') \approx W(x)\delta(x - x')$. We see that in the EDX case the maximum signal for the C K shell occurs when the probe is on the C column.

Let us now investigate the role of the nonlocality of $W(x, x')$ (which is purely real) more closely. The plot of $W(x, x')$ for the EELS case shown in Fig. 3(a) shows that, besides being ''delocalized'' along the diagonal, the potential has significant contributions off the diagonal. This should be contrasted with $W(x, x')$ for the EDX case, which is shown in Fig. 3(b), where it is evident that $W(x, x') \approx W(x)\delta(x - x')$. For the EELS case the potential $W(x, x')$ ''interacts'' strongly off the diagonal with the quantity $\Re[\psi_0^*(R, x, z)\psi_0(R, x', z)]$ in the integrand of Eq. (12), shown in Fig. 3(c) for a depth $z = 25$ Å and probe position above a Si column, as can be seen in the plot of $\Re[\psi_0^*(R, x, z)W(x, x')\psi_0(R, x', z)]$ in Fig. 3(d) ($\Im[\psi_0^*(R, x, z)W(x, x')\psi_0(R, x', z)]$ integrates to zero). By contrast, see Fig. 3(e), for EDX the potential interacts on and near the diagonal where $\psi_0^*(R, x, z)\psi_0(R, x', z) \approx |\psi_0(R, x, z)|^2$. At a depth $z = 50$ Å the function $\Re[\psi_0^*(R, x, z)\psi_0(R, x', z)]$, shown in Fig. 3(f), has spread both along and off the diagonal and the nonlocal EELS

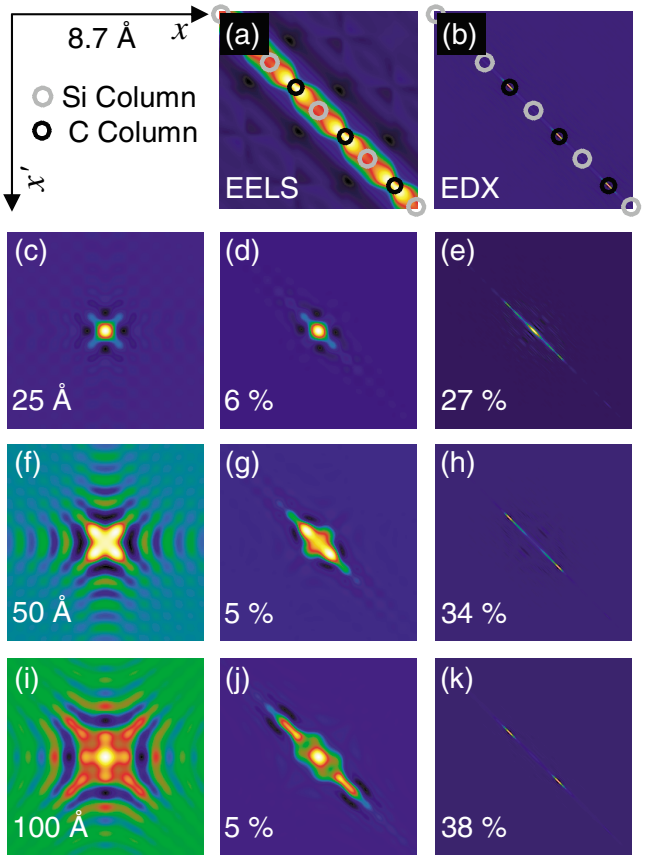

FIG. 3 (color online). (a) The effective nonlocal potential $W(x, x')$, used in calculating the results shown in Fig. 2(c). (b) $W(x, x')$ for the image shown in Fig. 2(d). (c) $\Re[\psi_0^*(R, x, z)\psi_0(R, x', z)]$ at a depth $z = 25$ Å for the probe situated on the Si column. (d) $\Re[\psi_0^*(R, x, z)W(x, x')\psi_0(R, x', z)]$ for the EELS case and (e) the EDX case or these conditions. Similar results to (c), (d), and (e) are shown in (f), (g), and (h) for a depth of $z = 50$ Å, and (i), (j), and (k) for a depth of $z = 100$ Å. The percentages indicate the percentage contribution that the diagonal values of the integrand make to the cross section at the relevant depth.

potential once again interacts strongly with the product of wave functions off the diagonal, as can be seen in Fig. 3(g). Although the interaction in the EDX case is evident over a greater distance along the diagonal (increasing cross talk), Fig. 3(h) shows that it is even more confined to the diagonal. These trends are maintained for a depth $z = 100$ Å, as can be seen in Figs. 3(i)–3(k).

In Table. I we show the depth-integrated contribution to the image for different depths for the probe above Si and C. The contributions are shown relative to assuming that the integrated contribution at 100 Å is unity when the probe is above a C column. The numbers in brackets indicate the percentage of the cross section that is derived from the principal diagonal (i.e., strictly local contributions). If we look at the contributions from additional diagonal lines of pixels, moving out from the principal diagonal, in Figs. 3(j) and 3(k) then we find that in the EELS case we need to move out about 1.2 Å on either side of the diagonal before we obtain essentially all of the contributions to the cross section. In the nearly local EDX case this is achieved within 0.2 Å of the diagonal.

TABLE I. Summary of the depth-integrated contributions to the cross section with the probe located above the Si and C columns. Results are shown for both EELS and EDX, with the contribution on the C column at 100 Å normalized to one. The percentage of the signal derived from the diagonal is shown in brackets for each case.

Depth (Å)	EELS		EDX	
	Si	C	Si	C
25	0.22 (6.9)	0.27 (7.9)	0.09 (25.3)	0.38 (44.2)
50	0.49 (6.3)	0.53 (7.7)	0.21 (28.5)	0.65 (42.6)
75	0.83 (5.9)	0.77 (7.6)	0.38 (32.4)	0.82 (40.8)
100	1.18 (5.6)	1.00 (7.6)	0.57 (34.6)	1.00 (39.8)

We have demonstrated that imaging based on an effective nonlocal interaction with the specimen can lead to unexpected results. The kernel representing the inelastic scattering allows a signal to be obtained from a site where the probe has negligible intensity. This result has major implications for imaging in STEM based on low-loss EELS. The usual assumptions of locality of the imaging process are no longer valid, meaning that there is no longer a simple connection between a signal at a given probe position and the location of atoms giving rise to that signal.

L. J. Allen and M. P. Oxley acknowledge support by the Australian Research Council. We thank S. D. Findlay for several helpful discussions.

[1] J. S. Bell, Physics (Long Island City, N.Y.) **1**, 195 (1964).
[2] L. J. Allen *et al.*, Phys. Rev. Lett. **91**, 105503 (2003).
[3] M. Valera *et al.*, Phys. Rev. Lett. **92**, 095502 (2004).
[4] H. Yoshioka, J. Phys. Soc. Jpn. **12**, 618 (1957).
[5] L. J. Allen and T. W. Josefsson, Phys. Rev. B **52**, 3184 (1995).
[6] M. P. Oxley and L. J. Allen, Phys. Rev. B **57**, 3273 (1998).
[7] M. P. Oxley and L. J. Allen, Acta Crystallogr. Sect. A **57**, 713 (2001).
[8] A. P. Young and P. Rez, J. Phys. C **8**, L1 (1975).
[9] L. J. Allen *et al.*, Ultramicroscopy **96**, 47 (2003).
[10] E. J. Kirkland, *Advanced Computing in Electron Microscopy* (Plenum, New York, 1998).